The effect of laser-assisted diamond turning (Micro-LAM) on the underlying surface structure of selected IR crystals

Hossein Shahinian[1], Jayesh Navare[1], Dmytro Zaytsev[1], Sai Kode[1], Deepak Ravindra[1]
[1]Micro-LAM Inc
5960 S Sprinkle Rd
Portage, Michigan, USA

INTRODUCTION

In this paper we present the influence of, laser assisted diamond turning, i.e., μ-LAM process on the subsurface residual stresses of infrared (IR) crystals. The μ-LAM process uses the emission of laser light during single point diamond turning (SPDT) of optical components [1]. Conventional diamond machining centers can produce surfaces with low roughness values (<5 nm RMS), and form accuracy of 100 nm – 200 nm peak to valley (PV) [2, 3]. They key principle behind the fabrication of parts with such tight tolerances, is the use of ultra-precise and rigid machines that use single crystal diamond as their cutting tools. The μ-LAM process, leverages the laser light propagated through the single crystal diamond tool and on the cutting edge of the tool. The laser effectively induces heat "softening" to the material being cut, thus facilitating the cutting process [4, 5].

The SPDT has been an enabling technology in production for freeform and aspherical optics [6, 7]. Freeform optics have received a wide traction for several optical applications, such as imaging optics [8, 9], illumination optics [10], etc. The optics generated by SPDT would require additional post finishing step, for having acceptable performance in the visible light regime [11-14]. However, those restriction are much looser when dealing with IR optics. Thus, the SPDT process is of great value for such optics.

Many articles, published previously by the Micro-LAM team, have demonstrated the positive effect of the laser on the cutting process in improving the surface finish of the parts produced as such. To better understand the key reasons behind the enhanced performance of a diamond tool using the μ-LAM system, an investigation on the underlaying surface residual stresses of the cut materials with and without the μ-LAM system, is proposed.

Studying the residual stresses of metallic and non-metallic components have been undertaken by different methods in the past [15, 16]. One of the most common approaches in doing so is the use of the X-ray diffractometer (XRD). The application of XRD in measuring residual stresses has been shown in several articles [17-20]. In this article the focus is not on the calculation of the residual stresses of the parts per se, but the goal is to compare the extent to which the residual stresses on the optics fabricated with and without the μ-LAM process differ.

The comparison is done for two different IR crystals that have wide applications within the optics community. The first sample is made of single crystal silicon (Si), and the second is a polycrystalline zinc sulfide (ZnS). Both materials can be cut in a ductile manner with single crystalline diamond tools [21].

EXPERIMENTAL METHOD

To compare the residual stresses induced during fabrication of ZnS and Si, planar samples were used. The testing includes diamond turning of the surface of the samples with and without the μ-LAM system. The experiments are conducted under identical spindle RPM and feedrates for the respective materials. The cuts are performed on a 2-axis ultraprecision lathe, a Precitech Nanoform 250. The machined samples are then measured on an XRD instrument post the cutting.

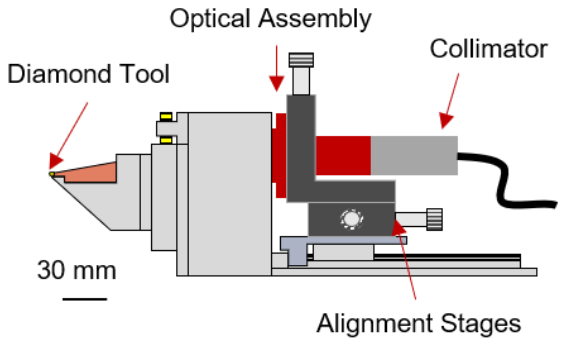

FIGURE 1. The Optimus$_{T+1}$ tool post

Optimus$_{T+1}$ tool post

The tool post is a proprietary product of the Micro-LAM team, whereby the laser is delivered to the cutting zone. **Error! Reference source not found.** depicts a sketch of the Optimus$_{T+1}$. The laser used has a wavelength of 1064 nm, and the beam is focused near the cutting edge of the diamond tool. The diamond material has a transmission of 70% for the 1064 nm wavelength. This implies that most of the laser power is transmitted through the tool towards the cutting edge. The laser light is then guided such that the beam exits the diamond at the cutting edge of the tool. The transmitted laser through the tool "softens" the workpiece material as a result of the heat produced from the absorption of the laser radiation in a very localized fashion. This softening of the material facilitates the cutting process, thereby reducing the amount of tool wear induced during diamond turning. The schematics of the μ-LAM process in action is depicted in FIGURE 2.

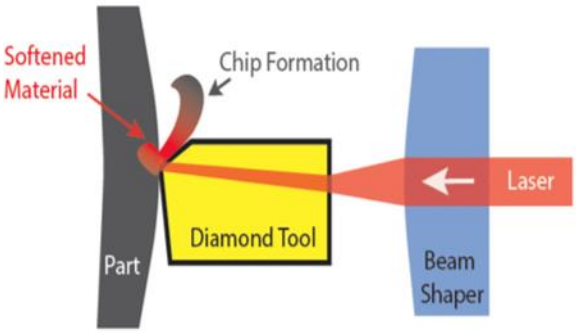

FIGURE 2. The transmission of the laser through the diamond too and the material "softening"

Test samples

The planar Si and ZnS, samples were diamond turned prior to the testing to ensure both samples had similar surface texture before the experiments. Table 1 outlines the dimensions of the used samples.

Table 1. Test sample information

Material	Dimension	Initial surface
Si	∅28 mm × 5 mm	Diamond turned
ZnS	∅25 mm × 5 mm	Diamond turned

Diamond cutting tools

The cutting tools used were made of single crystal synthetic diamonds. The tools were designed in such way that a path for the transmission of the laser was available. The tools were fabricated by K&Y Diamond®. The negative rake angle of the tool was necessary. As investigated by many researchers the negative rake angle provides a better opportunity for the ductile cutting of brittle materials [22].

Table 2. Diamond tool information

Tool	Rake angle (°)	Nose radius (mm)	Cutting height (mm)
1	-35	0.3	1.05
2	-35	0.3	1.17
3	-35	0.5	1.11
4	-35	0.5	1.09

Diamond turning conditions

The testing conditions for the samples were opted based on the information available in the literature [23]. The diamond cutting conditions for Si and ZnS can be found in tables 3, 4 respectively.

Table 3. Cutting conditions for Si samples

Cut	RPM	Feed (μm/rev)	DOC (μm)
a	2000	3	6
b	2000	2	6
c	2000	1.5	6

Table 4. Cutting conditions for ZnS

Cut	RPM	Feed (μm/rev)	DOC (μm)
α	4000	0.75	6
β	4000	0.5	4
δ	4000	0.375	2

Four tests on the samples were conducted. Each sample underwent the cutting sequences outlined in table 3 and table 4 for their respective materials. Table 5 lists the four conducted experiments.

Table 5. Cutting tests with and without the μ-LAM system

Test	Cuts	Tool	Laser power (W)
Si-1	a, b, c	1	0
Si-2	a, b, c	2	2.7
ZnS-1	α, β, δ	3	0
ZnS-2	α, β, δ	4	2.7

The emission of the laser through the diamond is measured with an Ophir Optronics® F150A-BB-26-PPS power meter. FIGURE 3(a) shows the scattered footprint of the laser on a digital camera. FIGURE 3(b) shows the transmitted laser power measured with the power meter.

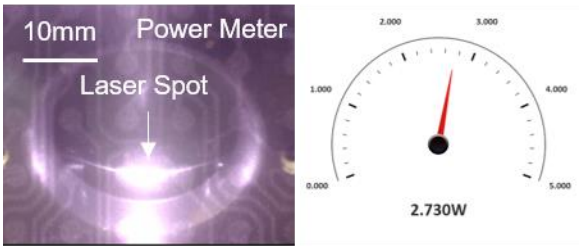

(a) (b)

FIGURE 3. (a) scattered laser footprint 8 mm away from the tool tip (b) measured laser power at that location

Metrology

Each workpiece was examined in two ways. The surfaces of the samples were measured under a scanning white light interferometer (SWLI), Taylor Hobson® Talysurf CCI. The instrument specifics as well as the processing operations applied to the raw data can be found in Table 6.

Table 6. SWLI instrument information

Hardware	Processing
Taylor Hobson Talysurf (CCI)	Best fit 4th order Chebyshev removed
20× Mirau objective 1024 × 1024 detector	Metric: RMS of the data i.e. Sq

The XRD measurements of the parts were acquired on a third generation Empyrean® diffractometer. The measurement was done using the gonio axis, and the instrument information can be found in Table 7.

Table 7. XRD measurement information

Diffractometer parameter	value
$K_{\alpha 1}$ wavelength	1.540598 Å
$K_{\alpha 2}$ wavelength	1.544426 Å
Generator voltage	45 V
Tube current	40 A
Gonio scan step size	0.002°

RESULTS

The cutting tests of Si-1, Si-2, ZnS-1, and ZnS-2, (see Table 5 for the tests), were done on four different samples. The spindle was balanced in each test to less than 1 nm PV deviations in the spindle position. In each test the surface of the samples were measured using the SWLI and XRD instruments.

Interferometric measurements

FIGURE 4(a), (b) depict the SWLI interferogram of the Si parts cut with and without the μ-LAM system. The RMS roughness (Sq) values were measured to be nearly the same. However, it should be noted that the surface cut with conventional diamond turning, showed minute traces of brittle fracture near the center of the part. These brittle fracture zones are very common in cutting single crystal materials [21].

The measurement interferograms for the ZnS samples are depicted in FIGURE 5 (a), (b). Evident in the figure both surfaces show signs of pits and damage zones. Nevertheless, these damaged zones appear to be of higher severity on the sample produced with conventional diamond turning. This is confirmed by the higher surface roughness RMS value of the ZnS sample machined with conventional diamond turning.

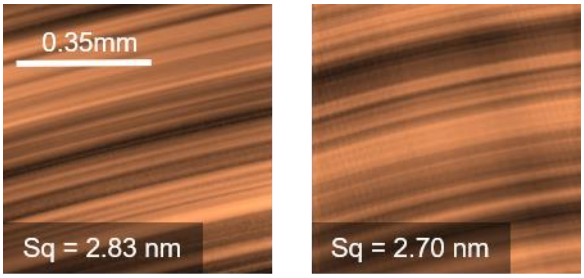

(a) (b)

FIGURE 4. interferometric imaging of Si samples (a) conventional (b) μ-LAM

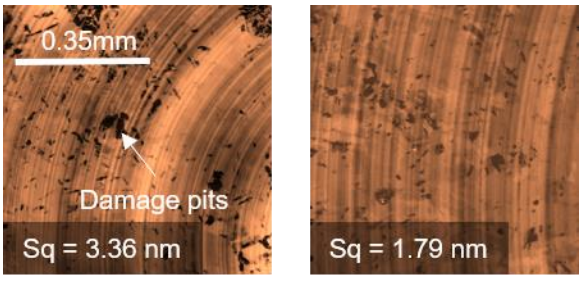

(a) (b)

FIGURE 5. Interferometric imaging of ZnS samples (a) conventional (b) μ-LAM

XRD measurements

To evaluate the relative residual stresses for the machined samples, XRD measurements were taken. To quantify the relative residual stresses, the full width at half maximum (FWHM), of the

diffraction peaks were calculated from the FWHM of the best fit Gaussian curves to the diffraction peaks. A narrower peak implies the presence of less residual stresses underneath the surface of the part. FIGURE 6 depicts the XRD measured data for the Si samples. The figure suggests a very distinct difference between the peaks of the samples at 68°. The FWHM for the Si-1 and Si-2 samples are 7.46°, and 0.05° respectively. These numbers suggest that the Si sample machined using the μ-LAM process has nearly 150 times smaller residual stresses than that processed with conventional diamond turning. The splitting of the peaks on the measurement for the surface made with the μ-LAM process is attributed to the slight difference of the $K_{\alpha 1}$ and $K_{\alpha 2}$ wavelengths of the diffractometer.

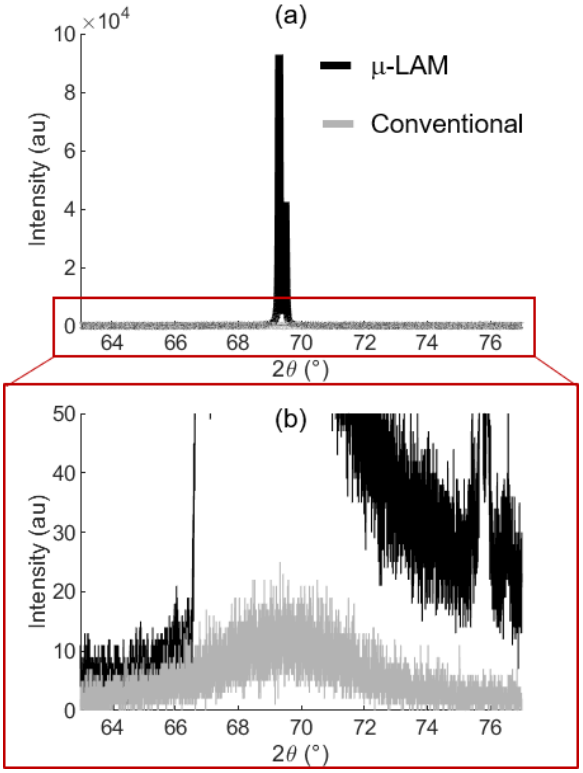

FIGURE 6. XRD peaks of single crystal Si diamond turned with and without μ-LAM; (a) Clear peak for the surface made with μ-LAM (b) zoomed on the peak of the Si made with conventional diamond turning

The same XRD measurements were done on the ZnS samples. Since the ZnS samples were made of a polycrystalline material, more than one diffraction peaks were scrutinized. FIGURE 7 shows the peaks that were studied. FIGURE 8 shows the FWHM of the peaks of ZnS-1 and ZnS-2 sample.

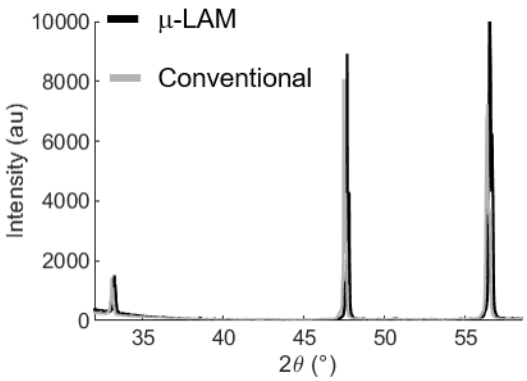

FIGURE 7. XRD measurements of the ZnS samples cut with and without the μ-LAM process

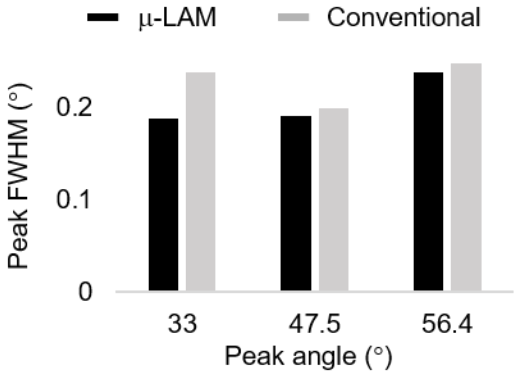

FIGURE 8. FWHM of diffraction peaks measured on ZnS samples

The FWHM of the peaks in FIGURE 8 suggests that the residual stresses are marginally lower for the sample machined with the μ-LAM process. That said, this data is inconclusive as the differences are within the uncertainty of the measurement of the XRD machine.

DISCUSSION

The results presented in the previous section are proof that the μ-LAM process does not deteriorate the mechanical integrity of the IR crystals with the addition of the laser to the diamond turning process. In case of Si, the laser has indeed greatly reduced the residual stresses of the part. From the lower residual stresses measured on the Si sample turned with the μ-LAM, it can be inferred that the surface and subsurface integrity of the Si can be greatly

improved using the μ-LAM process. A damage free surface and subsurface would intuitively require a cutting that happens in a more ductile fashion. Smaller residual stresses and therefore damage free sub surface, provides the opportunity to use those optics for high power IR lasers. A surface with high residual stresses is susceptible to fatigue fracture due to the extreme thermal gradients introduced by the lasers used.

The XRD measurement on the ZnS sample, doesn't show the significant reduction of the residual stresses within the ZnS material using the μ-LAM process. This could be attributed mainly to the much lower absorption rates of ZnS, compared to Si, in the 1064 nm wavelength regime. The absorption percentage of the laser power for the 1064 nm wavelength are 60% and 4%, for Si and ZnS respectively.

In addition, although the XRD data of the ZnS samples doesn't show a significant reduction in the residual stresses of the material, the SWLI interferograms clearly show a reduction in the pits and digs induced on the surface of the parts. This decrease in the surface defects, is speculated to be mainly due to a more ductile cutting of the ZnS using the μ-LAM process.

CONCLUSION AND FUTURE WORK

In summary of this paper, it was shown that the μ-LAM process enhances the ability of conventional diamond turning of IR crystals by producing mechanically more robust and damage free surfaces. While not reported here, our experimental evidence shows that the process can increase the diamond tool life at least twice as much as what is achievable in conventional diamond turning of Si.

As part of the future research efforts in the Micro-LAM team, this study approach will be pursued on additional IR crystals, as well as other hard and brittle materials to further understand and investigate the physics of the μ-LAM process.

ACKNOWLEDGEMENTS

We would like to acknowledge Dr. Pnina Ari-Gur for the XRD measurements of the samples. We would also like to thank Ms. Alyson Markos for her help in preparing the figures of the paper.

REFERENCES

1. Ravindra, D., *Ductile mode material removal of ceramics and semiconductors.* 2011.
2. Rhorer, R.L. and C.J. Evans, *Fabrication of optics by diamond turning.* Handbook of optics, 1995. **1**: p. 41.1-41.3.
3. To, S.S., V.H. Wang, and W.B. Lee, *Single Point Diamond Turning Technology*, in *Materials Characterisation and Mechanism of Micro-Cutting in Ultra-Precision Diamond Turning*. 2018, Springer. p. 3-6.
4. Ravindra, D., M.K. Ghantasala, and J. Patten, *Ductile mode material removal and high-pressure phase transformation in silicon during micro-laser assisted machining.* Precision engineering, 2012. **36**(2): p. 364-367.
5. Ravindra, D. and J. Patten, *Ductile regime single point diamond turning of quartz resulting in an improved and damage-free surface.* Machining Science and Technology, 2011. **15**(4): p. 357-375.
6. Zhang, X., Z. Li, and G. Zhang, *High performance ultra-precision turning of large-aspect-ratio rectangular freeform optics.* CIRP Annals, 2018.
7. Cheng, Y.-C., W.-J. Peng, H.-Y. Chou, and F.-Z. Chen. *Fabrication and measurement of freeform mirror for head-up display system*. in *Optical Fabrication, Testing, and Metrology VI*. 2018. International Society for Optics and Photonics.
8. Shahinian, H., T. Noste, N. Sizemore, C. Hovis, P. Shanmugam, N. Horvath, and D. Gurganos. *See-through smart glass with adjustable focus*. in *Digital Optics for Immersive Displays*. 2018. International Society for Optics and Photonics.
9. Huang, H. and H. Hua, *High-performance integral-imaging-based light field augmented reality display using freeform optics.* Optics Express, 2018. **26**(13): p. 17578-17590.
10. Wu, R., Z. Feng, Z. Zheng, R. Liang, P. Benítez, J.C. Miñano, and F. Duerr, *Design of Freeform Illumination Optics.* Laser & Photonics Reviews, 2018: p. 1700310.
11. Hull, T., M.J. Riso, J.M. Barentine, and A. Magruder. *Mid-spatial frequency matters: examples of the control of the power spectral density and what that means to the performance of imaging systems*. in *Infrared Technology and Applications XXXVIII*. 2012.

International Society for Optics and Photonics.
12. Chen, G., Y. Sun, F. Zhang, C. An, W. Chen, and H. Su, *Influence of ultra-precision flycutting spindle error on surface frequency domain error formation.* The International Journal of Advanced Manufacturing Technology, 2017. **88**(9-12): p. 3233-3241.
13. Shahinian, H., *Fiber Based Tools for Polishing Optical Materials*. 2018, The University of North Carolina at Charlotte.
14. Shahinian, H., M. Hassan, H. Cherukuri, and B.A. Mullany, *Fiber-based tools: material removal and mid-spatial frequency error reduction.* Applied optics, 2017. **56**(29): p. 8266-8274.
15. Almen, J.O. and P.H. Black, *Residual stresses and fatigue in metals*. 1963: McGraw-Hill.
16. Lu, J., *Handbook of measurement of residual stresses*. 1996: Fairmont Press.
17. Fitzpatrick, M., A. Fry, P. Holdway, F. Kandil, J. Shackleton, and L. Suominen, *Determination of residual stresses by X-ray diffraction.* 2005.
18. Klug, H.P. and L.E. Alexander, *X-ray diffraction procedures: for polycrystalline and amorphous materials.* X-Ray Diffraction Procedures: For Polycrystalline and Amorphous Materials, 2nd Edition, by Harold P. Klug, Leroy E. Alexander, pp. 992. ISBN 0-471-49369-4. Wiley-VCH, May 1974., 1974: p. 992.
19. Prevey, P.S., *X-ray diffraction residual stress techniques.* ASM International, ASM Handbook., 1986. **10**: p. 380-392.
20. Dufrenoy, S., T. Chauveau, I. Lemaire-Caron, R. Brenner, and B. Bacroix, *Comparison of 2 methodologies developed for the determination of residual stresses through X-ray diffraction: application to a textured hcp titanium alloy.* International Journal of Material Forming, 2018. **11**(3): p. 341-355.
21. Liu, H., W. Xie, Y. Sun, X. Zhu, and M. Wang, *Investigations on brittle-ductile cutting transition and crack formation in diamond cutting of mono-crystalline silicon.* The International Journal of Advanced Manufacturing Technology, 2018. **95**(1-4): p. 317-326.
22. Mir, A., X. Luo, K. Cheng, and A. Cox, *Investigation of influence of tool rake angle in single point diamond turning of silicon.* The International Journal of Advanced Manufacturing Technology, 2018. **94**(5-8): p. 2343-2355.
23. Abdulkadir, L.N., K. Abou-El-Hossein, A.I. Jumare, P.B. Odedeyi, M.M. Liman, and T.A. Olaniyan, *Ultra-precision diamond turning of optical silicon—a review.* The International Journal of Advanced Manufacturing Technology, 2018: p. 1-36.